Supplementary Information

Insights into the Multiple Effects of Oxygen Vacancies on CuWO$_4$ for Photoelectrochemical Water Oxidation

Wenlong Guo[a], Ya Wang[a], Xin Lian[b]*, Yao Nie[a], Shijia Tian[a], Shanshan Wang[a], Yun Zhou[a]*, Graeme Henkelman[c]

[a]*Chongqing Key Laboratory of Green Synthesis and Applications, College of Chemistry, Chongqing Normal University, Chongqing 401331, P. R. China*
[b]*College of Chemistry and Chemical Engineering, Chongqing University of Science and Technology, Chongqing, 401331, PR China*
[c]*Department of Chemistry and the Oden Institute for Computational Engineering and Sciences, The University of Texas, Austin, Texas 78712, United States*

E-mail address: daisylian0121@163.com (X Lian); yunzhou@cqnu.edu.cn (Y Zhou)

Film Synthesis and Characterization

All chemicals were obtained from commercial sources and used without further purification. The $CuWO_4$ films were synthesized according to the literature with some modifications.[1,2] Briefly, 0.4625 g of sodium tungstate was dissolved into 120 mL deionized water. Then, 10 mL of 1 M HCl and 0.1931 g oxalic acid were added and stirred to dissolved. Subsequently, 16 mL of the above solution was transferred into a Teflon-lined autoclave (20 mL) and a FTO glass substrate was placed diagonally in the autoclave. The FTO substrates were ultrasonically treated for 15 mins in acetone, ethanol, and water respectively. The autoclave was kept at 180 °C for 3 h and naturally cooled to room temperature. After the reaction, the FTO glass substrate with thin film was rinsed with water. 200 μL Cu^{2+} precursor solution (0.1208 g $Cu(NO_3)_2 \bullet 3H_2O$ dissolved in 5 mL acetic acid) coated the surface of this as-prepared film and then the film was annealed in air at 550 ℃ for 2 h with a heating rate of 2 ℃/min. The annealed film was soaked in 0.5 M HCl solution for 30 mins to remove the excess copper oxide. To introduce oxygen vacancies, the obtained $CuWO_4$ films were subsequently treated under a nitrogen atmosphere (1 bar, 50 sccm gas flow) at various temperatures for 3 hours. Nickel phosphate (Ni-Pi) was deposited on the $CuWO_4$ films according the literature.[20] Briefly, 0.5 mM $Ni(NO_3)_2$ was added into 0.1 M potassium phosphate buffer (pH 7) and then this mixture was sonicated for 30 mins to form a homogeneous suspension. Drop-casting method was used to deposit the Ni-Pi on $CuWO_4$ films and a 100 $μL/cm^2$ of the suspension was found to be the optimum load according to the PEC tests.

The phases of the synthesized films were determined using X-ray diffraction (XRD) measurements with Cu $K\alpha$ X-rays (SHIMADU). The morphologies of the films were obtained using a scanning electron microscope (SEM, FEI Inspect F50 (FSEM)). The light absorption properties were evaluated using UV-vis spectroscopy (SHIMADU). Vibration spectra were collected using a confocal Raman spectrometer (Saimofei DXR). The electron binding energy of Cu, W, O, Ni, and P elements were acquired with X-ray photoelectron spectroscopy (XPS, Escalab).

Electrochemical and Photoelectrochemical Measurements

Electrochemical and photoelectrochemical measurements were conducted in a three-electrode cell. In this cell, the working electrode is the $CuWO_4$ thin film, the counter electrode is a Pt sheet (99.95%, Chenhua), the reference electrode is a Ag/AgCl electrode in the saturated KCl (CHI111). The illumination source is a 300 W xenon lamp (PLS-SXE 300) with an AM1.5G filter. The illumination area of the film is 1 cm^2 and the light intensity of 100 mW/cm^2 was measured by a thermopile detector (FZ-A). The incident light impinges on the film surface. All electrochemical and photoelectrochemical measurements were conducted using an electrochemical workstation (CHI 760E).

The separation efficiency (η_{sep}) and injection efficiency (η_{inj}) of $CuWO_4$ and $CuWO_4$ (OV) photoanodes are calculated based on Eqs. (1) and (2) respectively,

$$\eta_{sep} = j_{Na_2SO_3} / j_{abs} \tag{1}$$

$$\eta_{inj} = j_{Na_2SO_4} / j_{Na_2SO_3} \tag{2}$$

where $j_{Na_2SO_3}$ is the photocurrent density of the photoanode tested in a 0.2 M Na_2SO_4 electrolyte with 1 M Na_2SO_3 as a hole scavenger; j_{abs} is the photocurrent density derived from the light absorption. $j_{Na_2SO_4}$ is the photocurrent density of the photoanode measured in a 0.2 M Na_2SO_4 solution.

The flat band potentials are investigated using Mott-Schottky measurements and determined using Eq. (3),

$$1/C^2 = (2/\varepsilon\varepsilon_o N_d)[V_a - V_{fb} - kT/e] \tag{3}$$

where C is the capacitance of the space charge layer; e is the electronic charge; ε is the dielectric constant; ε_o is the permittivity of free space; N_d is the carrier concentration; V_a is the applied potential; V_{fb} is the flat band potential; k is the Boltzmann constant; and T is the temperature. The carrier concentration is calculated from the slope of Mott-Schottky curves based on Eq. (4),[3]

$$N_d = \frac{2}{e_0 \varepsilon_0 \varepsilon} \left(\frac{dC^{-2}}{dV} \right) - 1 \tag{4}$$

where e_0 is the elemental charge; $\varepsilon = 83$ is applied as the dielectric constant of CuWO$_4$.[4]

The transport time of the photogenerated electron from the surface to the substrate is evaluated by a controlled intensity modulated photocurrent spectrometer (CIMPS) based on the Eq. (5),[5-7]

$$\tau = 1/(2\pi f_{min}) \tag{5}$$

where τ is the transport time and f_{min} is the frequency corresponding to the lowest point of the imaginary components.

Computational Details

Vienna ab initio simulation package (VASP)[8-10] was used to conduct the DFT calculations with a plane wave basis set and a cut-off energy of 420 eV.[11,12] Electronic-correlation energies were calculated through the generalized gradient approximation functional of the Perdew–Burke–Ernzerhof form.[13,14] A (4×3×1) Monkhorst-Pack grid was used for Brillouin-zone integration for the (1×2) surface unit cell of the CuWO$_4$ (010) surface.[15] The surface was modeled using a slab geometry with four layers. In this structure, the top two layers were free to relax until all force components dropped below 0.01 eV/Å, while the bottom layers were constrained to bulk positions. 15 Å vacuum was used to separate the periodic images in the direction perpendicular to the surface. The climbing-image nudged elastic band (CI-NEB) method[16] was used to search for transition states (TSs) of the water dehydrogenation reactions. The H$_2$O adsorption energies (E_{ads}) were calculated as Eq. (6),

$$E_{ads} = E_{CuWO_4/H_2O} - (E_{CuWO_4} + E_{H_2O}) \tag{6}$$

where E_{CuWO_4/H_2O} is the total energy of the CuWO$_4$-H$_2$O system, E_{H_2O} is the energy of an isolated water molecule, and E_{CuWO_4} is the energy of the CuWO$_4$ substrate without water adsorption. The activation barriers were used to calculate the rate constants of the elementary reactions based on the Eyring equation (7):

$$k = \frac{k_b T Q^{TS}}{h \quad Q} e^{-\frac{E_a}{k_b T}}$$

(7)

where k is the reaction rate constant; h is Planck's constant; k_b is Boltzmann's constant; T is the reaction temperature; Q is the partition functions of the ground states; Q^{TS} is the partition functions of the transition states; E_a is the activation barrier; and $\dfrac{k_b T Q^{TS}}{h \quad Q}$ is the prefactor A which was taken as 10^{13} s^{-1} for simplicity.
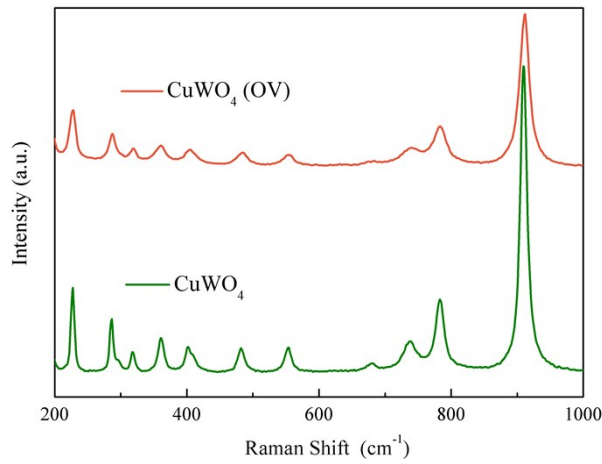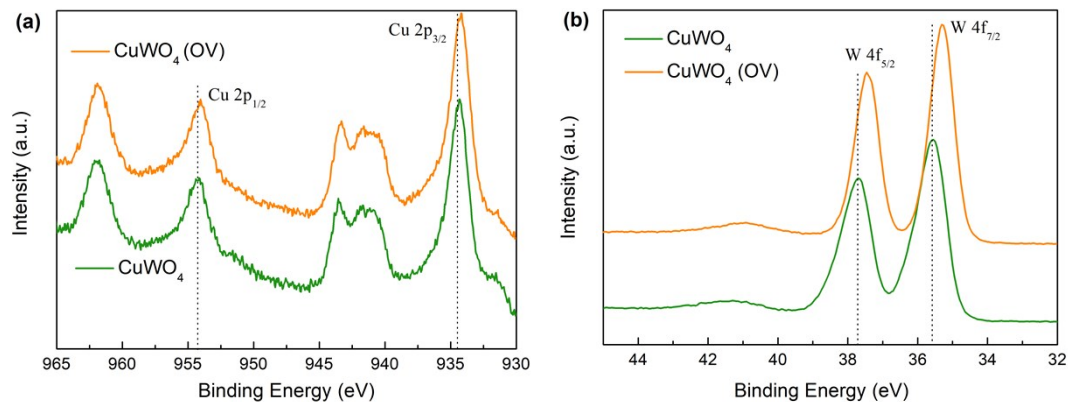

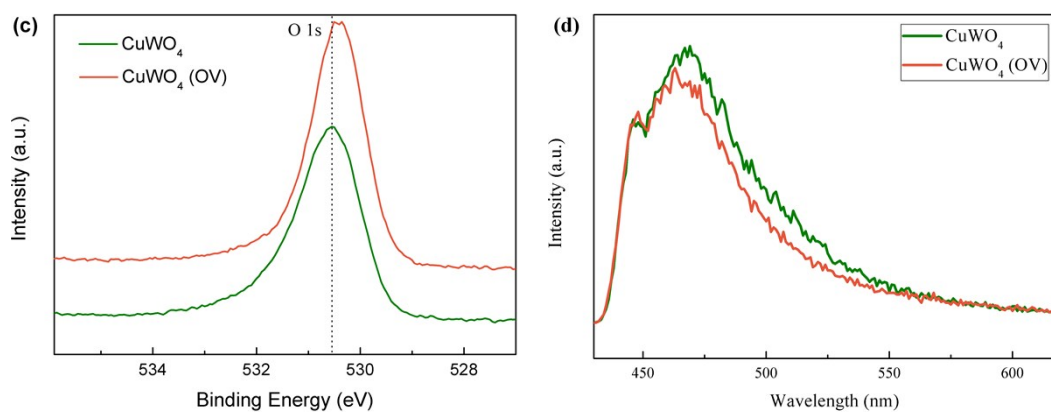**Figure S1.** Raman spectra of CuWO$_4$ and CuWO$_4$ (OV) films.

Figure S2. XPS spectra of (a) Cu 2p, (b) W4f, and (c) O 1s collected from CuWO$_4$ and CuWO$_4$ (OV) films. (d) Photoluminescence spectra of CuWO$_4$ and CuWO$_4$ (OV) films.

Discussion of Figures S1 and S2: Vibration spectra of CuWO$_4$ films before and after the N$_2$ treatment at 300 ℃ for 3 h are shown in Figure S1. It shows that, compared to the pristine CuWO$_4$, the intensity of the Raman peaks decreases and the width broadens for the post-annealed CuWO$_4$ film. These changes reveal the decline of the crystallinity and the formation of defects, demonstrating the generation of oxygen vacancies. This phenomenon is also observed in previous work.[17] XPS measurements were conducted to further verify the existence of the oxygen vacancies for the CuWO$_4$ film post-annealed in N$_2$ atmosphere (Figure S2). The binding energies of Cu 2p, W 4f, and O1s electrons of the post-annealed CuWO$_4$ film all become lower than those of the non-treated CuWO$_4$. This suggests that the shielding effect of the outer electrons enhances and the chemical valences of elements are reduced, confirming the generation of oxygen vacancies.[17,18] Compared to CuWO$_4$, the photoluminescence emission spectrum of CuWO$_4$ (OV) is weaker. This is due to the increase of the nonradioactive recombination caused by the oxygen vacancies on the surface.[21]
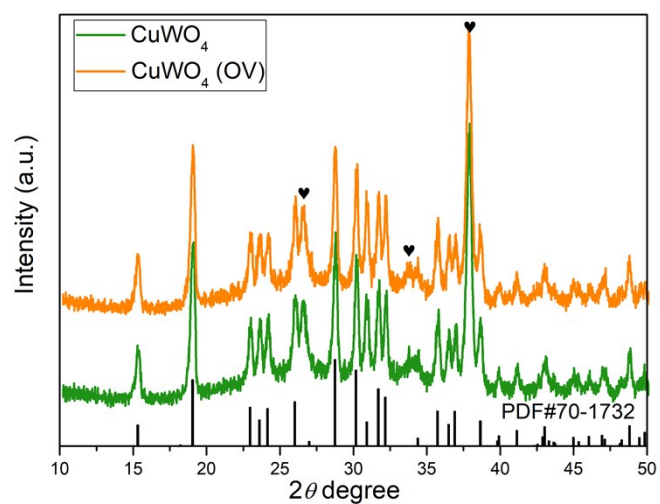
Figure S3. XRD patterns of (green curve) $CuWO_4$ and (orange curve) $CuWO_4$ (OV) films (PDF#70-1732). The heart-shaped symbols indicate the characteristic peaks of the substrate (SnO_2).
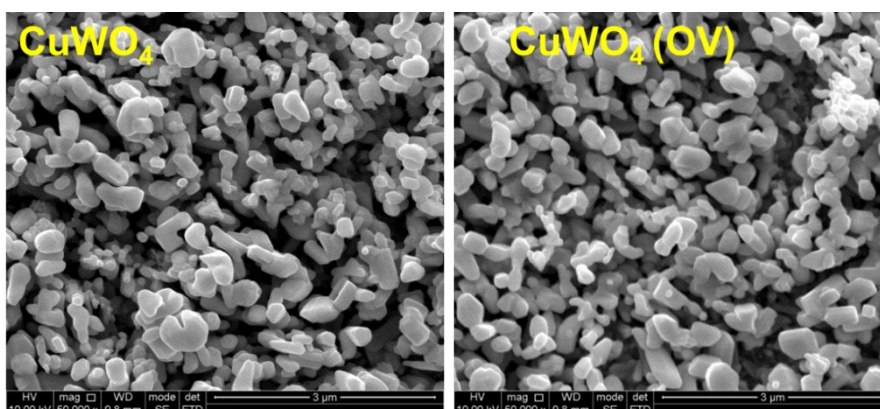

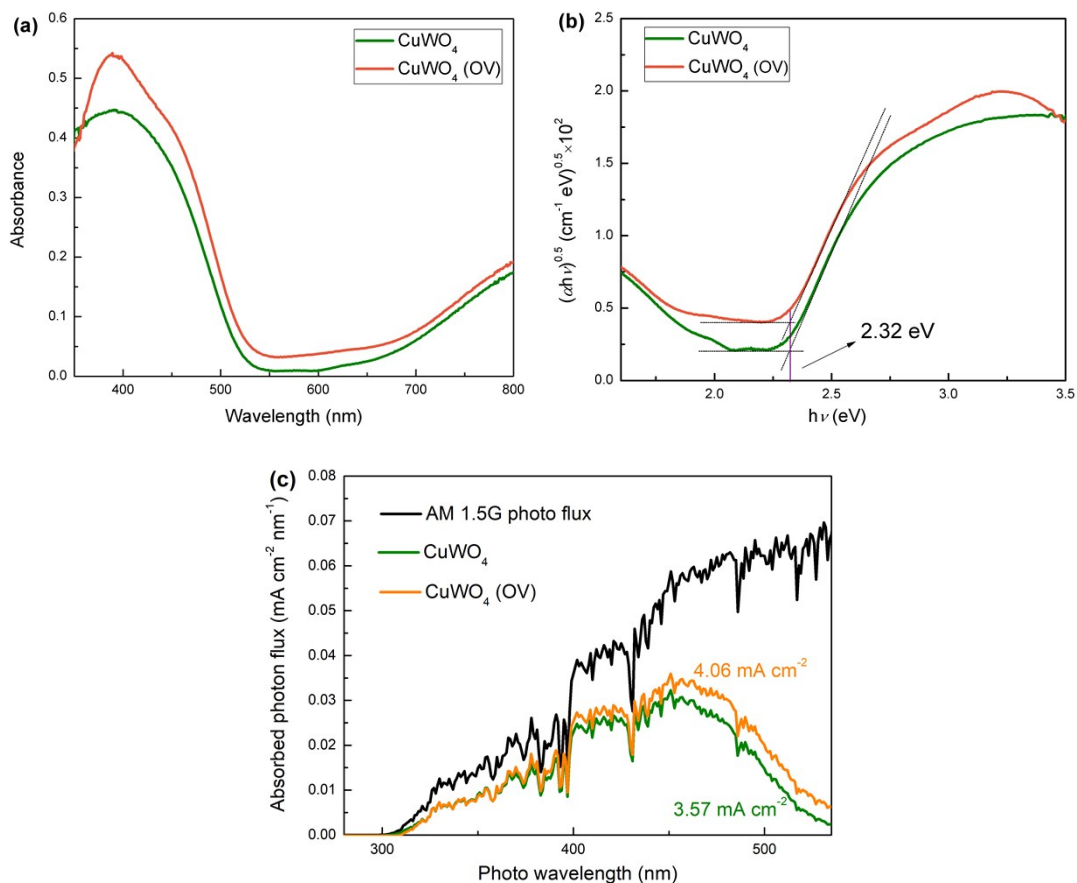**Figure S4.** Typical morphologies of $CuWO_4$ and $CuWO_4$ (OV) thin films.

Figure S5. (a) Absorbance spectra of CuWO$_4$ and CuWO$_4$ (OV) thin films and the derived (b) Tauc plot; (c) Absorbed photon flux of CuWO$_4$ and CuWO$_4$ (OV) films.
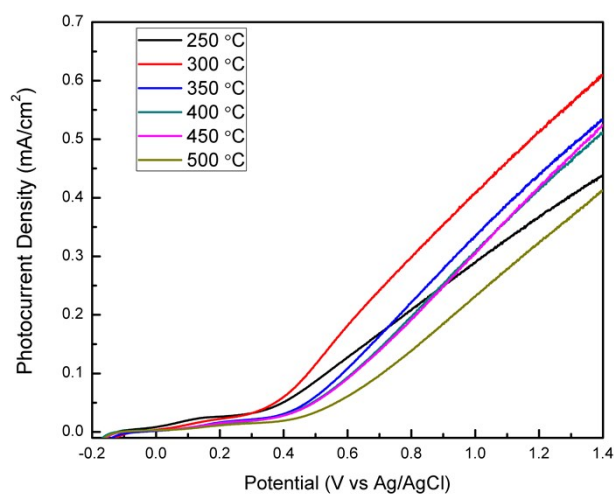

Figure S6. PEC performances of CuWO$_4$ films post-annealed in the N$_2$ atmosphere at various temperatures for 3 h.
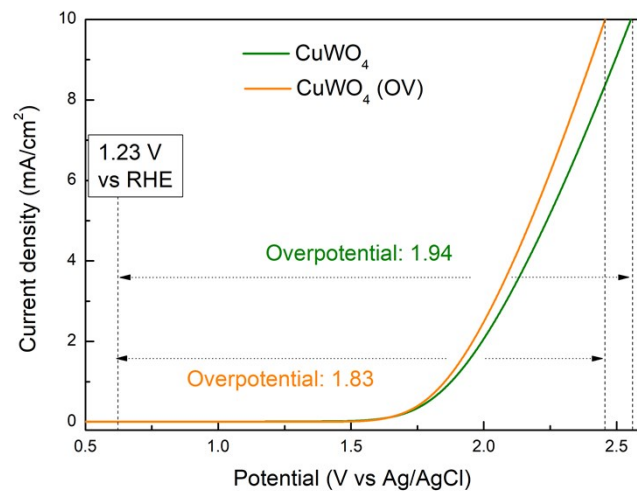
Figure S7. LSV curves of CuWO$_4$ and CuWO$_4$ (OV) films tested in 0.2 M Na$_2$SO$_4$ electrolyte in dark.
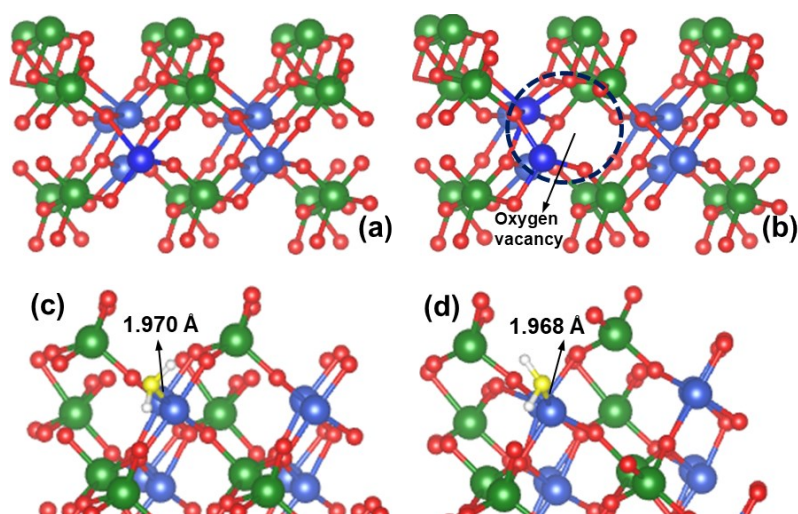

Figure S8. Optimized structures of (010) surfaces for (a) CuWO$_4$ and (b) CuWO$_4$ with oxygen vacancies. Optimized structures of (c) CuWO$_4$ and (d) CuWO$_4$ with oxygen vacancies adsorbed with a water molecule. Cu, W, and O are blue, green, and red spheres, respectively. The adsorbed O and H atoms are yellow and white, respectively.

Discussion of Figures S8:

Optimized structures of the CuWO$_4$ (010) surface with and without oxygen vacancy

(OV) are shown in Figures S8a and b. The OV is located on the outermost oxygen layer in the crystal lattice and connected by one Cu atom and one W atom with a coordination number of 2. It is known that TiO_2 can easily generate OVs; the formation energy of an OV is about 3.55 eV.[19] In contrast, the formation energy of an OV is 1.44 eV on the $CuWO_4$ (010) facet which is smaller than that on the TiO_2 (110) facets, indicating that the OV can also be easily formed on the $CuWO_4$ (010) facet. The structures of a water molecule adsorbed on the $CuWO_4$ (010) surface with and without an OV are shown in Figures S8c and d. On both of these surfaces, H_2O approaches the surface by connecting with the terminal Cu through the O end, which is the most stable configuration. The calculated Cu-O distance is 1.970 and 1.968 Å on the perfect and OV-containing surfaces, respectively. The adsorption energy of H_2O on the $CuWO_4$ and $CuWO_4$ with OV is -1.19 and -1.54 eV respectively, implying that the interaction between H_2O and the surface containing an OV is stronger than that between H_2O and the stoichiometric surface.

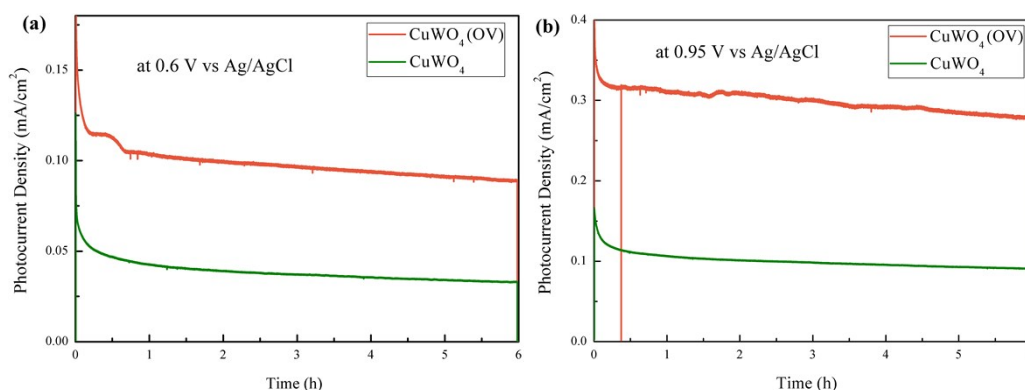**Figure S9.** PEC water oxidation stabilities for $CuWO_4$ and $CuWO_4$ (OV) tested in 0.2 M Na_2SO_4 electrolyte at (a) 0.6 and (b) 0.95 V vs Ag/AgCl for 6 h. The illumination is AM 1.5G simulated solar light with an intensity of 100 mW/cm^2.
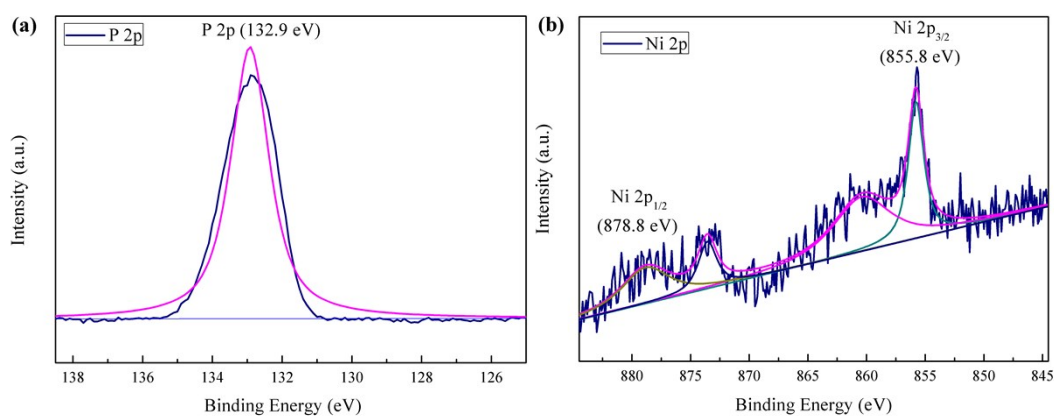
Figure S10. XPS spectra of the CuWO$_4$/Ni-Pi film for (a) P 2p and (b) Ni 2p. The binding energies in the XPS spectra were calibrated using the C 1s (284.8 eV).

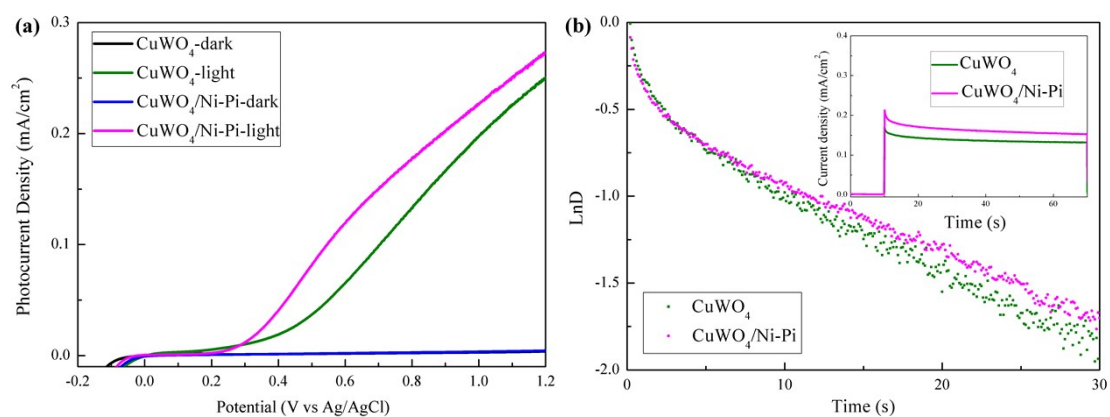**Figure S11.** (a) LSV curves of CuWO$_4$ and CuWO$_4$/Ni-Pi tested in 0.2 M Na$_2$SO$_4$ electrolyte under AM 1.5G illumination (100 mW/cm^2). (b) Normalized plots of the current-time dependence of the anodic transients for CuWO$_4$ and CuWO$_4$/Ni-Pi films. The inset is the transient photocurrent responses of CuWO$_4$ and CuWO$_4$/Ni-Pi films measured at 0.9 V vs Ag/AgCl in 0.2 M Na$_2$SO$_4$ electrolyte.

Table S1. The values of the equivalent circuit elements in the fitted Nyquist plots of Fig. 3a.

Sample	R_s (Ω)/error (%)	CPE-T (F)/ error (%)	CPE-P / error (%)	R_{ct} (Ω)/error (%)
$CuWO_4$	51.13/0.64	6.92×10^{-5}/2.61	0.83/0.60	1795/2.67
$CuWO_4$(OV)	44.23/0.85	6.39×10^{-5}/3.60	0.83/0.78	1190/2.60

Table S2. Reaction rate constants (s^{-1}) of elementary reactions for H_2O dehydrogenation on the (010) surfaces of $CuWO_4$ and $CuWO_4$ with oxygen vacancies (OV).

Elementary reaction	$CuWO_4$		$CuWO_4$ with OV	
	T (298.15 K)	T (318.15 K)	T (298.15 K)	T (318.15 K)
$*OH_2 \rightarrow *OH + *H$	2.10×10^{-4}	2.35×10^{-3}	5.17×10^{1}	2.65×10^{2}
$*OH + *H \rightarrow *O + 2*H$	8.77×10^{-9}	1.85×10^{-7}	5.57×10^{4}	1.84×10^{5}

References

(1) Rodríguez-Gutierrez, I.; Djatoubai, E.; Rodríguez-Perez, M.; Su, J. Z.; Rodríguez-Gattorno, G.; Vayssieres, L.; Oskam, G. Photoelectrochemical Water Oxidation at FTO|WO$_3$@CuWO$_4$ and FTO|WO$_3$@CuWO$_4$|BiVO$_4$ Heterojunction Systems: An IMPS Analysis. *Electrochim. Acta* **2019**, *308*, 317-327.

(2) Liu, Y.; Zhao, L.; Su, J.; Li, M.; Guo, L. Fabrication and Properties of a Branched (NH$_4$)$_x$WO$_3$ Nanowire Array Film and a Porous WO$_3$ Nanorod Array Film. *ACS Appl. Mater. Interfaces.* **2015**, *7*, 3532-3538.

(3) Chen, Z.; Jaramillo, T. F.; Deutsch, T. G.; Kleiman-Shwarsctein, A.; J.Forman, A.; Gaillard, N.; Garland, R.; Takanabe, K.; Heske, C.; Sunkara, M. Accelerating Materials Development for Photoelectrochemical Hydrogen Production: Standards for Methods, Definitions, and Reporting Protocols. *J. Mater. Res.* **2010**, *25*, 3-16.

(4) Arora, S. K.; Mathew, T. Dielectric Studies of CuWO$_4$ Crystals. *Phys. Status Solidi A* **1989**, *116*, 405-413.

(5) Oekermann, T.; Zhang, D. S.; Yoshida, T.; Minoura, H. Electron Transport and Back Reaction in Nanocrystalline TiO_2 Films Prepared by Hydrothermal Crystallization. *J. Phys. Chem. B* **2004**, *108*, 2227-2235.

(6) Zhang, Y. P.; Li, Y.; Ni, D. Q.; Chen, Z. W.; Wang, X.; Bu, Y. Y.; Ao, J. P. Improvement of $BiVO_4$ Photoanode Performance During Water Photo-Oxidation Using Rh-Doped $SrTiO_3$ Perovskite as a Co-Catalyst. *Adv. Funct. Mater.* **2019**, *29*, 1902101.

(7) Xiong, Y. L.; Yang, L.; He, H. C.; Wan, J.; Xiao, P.; Guo, W. L. Enhanced Charge Separation and Transfer by Bi_2MoO_6@$Bi_2Mo_2O_9$ compound using SILAR for photoelectrochemical water oxidation. *Electrochimi. Acta* **2018**, *264*, 26-35.

(8) Kresse, G.; Hafner, J. Ab Initio Molecular Dynamics for Liquid Metals. *Phys. Rev. B: Condens. Matter Mater. Phys.* **1993**, *47*, 558-561.

(9) Kresse, G.; Hafner, J. Ab Initio Molecular-Dynamics Simulation of The Liquid-Metal−Amorphous-Semiconductor Transition in Germanium. *Phys. Rev. B: Condens. Matter Mater. Phys.* **1994**, *49*, 14251-14269.

(10) Kresse, G.; Furthmuller, J. Efficiency of Ab-Initio Total Energy Calculations for Metals and Semiconductors Using a Plane-Wave Basis Set. *Comput. Mater. Sci.* **1996**, *6*, 15-50.

(11) Blöchl, P. E. Projector Augmented-Wave Method. *Phys. Rev. B: Condens. Matter Mater. Phys.* **1994**, *50*, 17953-17979.

(12) Kresse, G.; Joubert, D. From Ultrasoft Pseudopotentials to The Projector Augmented-Wave Method. *Phys. Rev. B: Condens. Matter Mater. Phys.* **1999**, *59*, 1758-1775.

(13) Kresse, G.; Furthmuller, J. Efficient Iterative Schemes for ab initio Total-Energy Calculations Using a Plane-Wave Basis Set. *Phys. Rev. B: Condens. Matter Mater. Phys.* **1996**, *54*, 11169-11186.

(14) Perdew, J. P.; Burke, K.; Ernzerhof, M. Generalized Gradient Approximation Made Simple. *Phys. Rev. Lett.* **1996**, *77*, 3865-3868.

(15) Monkhorst, H. J.; Pack, J. D. Special Points for Brillouin-Zone Integrations. *Phys. Rev. B* **1976**, *13*, 5188-5192.

(16) Henkelman, G.; Uberuaga, B. P.; Jonsson, H. A Climbing Image Nudged Elastic Band Method for Finding Saddle Points and Minimum Energy Paths. *J. Chem. Phys.* **2000**, *113*, 9901-9904.

(17) Tang, Y. L.; Rong, N.; Liu, F. L.; Chu, M. S.; Dong, H. M.; Zhang, Y. H.; Xiao, P.

Enhancement of the Photoelectrochemical Performance of $CuWO_4$ Films for Water Splitting by Hydrogen Treatment. *Appl. Surf. Sci.* **2016**, *361*, 133-140.

(18) Ma, Z. L.; Linnenberg, O.; Rokicinska, A.; Kustrowski, P.; Slabon, A. Augmenting the Photocurrent of $CuWO_4$ Photoanodes by Heat Treatment in the Nitrogen Atmosphere. *J. Phys. Chem. C* **2018**, *122*, 19281-19288.

(19) Wu, X.; Selloni, A.; Nayak, S. K. First Principles Study of CO Oxidation on TiO_2 (110): The Role of Surface Oxygen Vacancies. *J. Chem. Phys.* **2004**, *120*, 4512-4516.

(20) Xiong, X. Q.; Fan, L. Y.; Chen, G. H.; Wang, Y.; Wu, C. L.; Chen, D.; Lin, Y.; Li, T. D.; Fu, S.; Ren, S. B. Boosting Water Oxidation Performance of $CuWO_4$ Photoanode by Surface Modification of Nickel Phosphate. *Electrochim. Acta* **2019**, *328*, 135125.

(21) Choudhury, B.; Choudhury, A. Oxygen Defect Dependent Variation of Band Gap, Urbach Energy and Luminescence Property of Anatase, Anatase–Rutile Mixed Phase and of Rutile Phases of TiO_2 Nanoparticles. *Physica E: Low-dimensional Systems and Nanostructures* **2014**, *56*, 364-371.